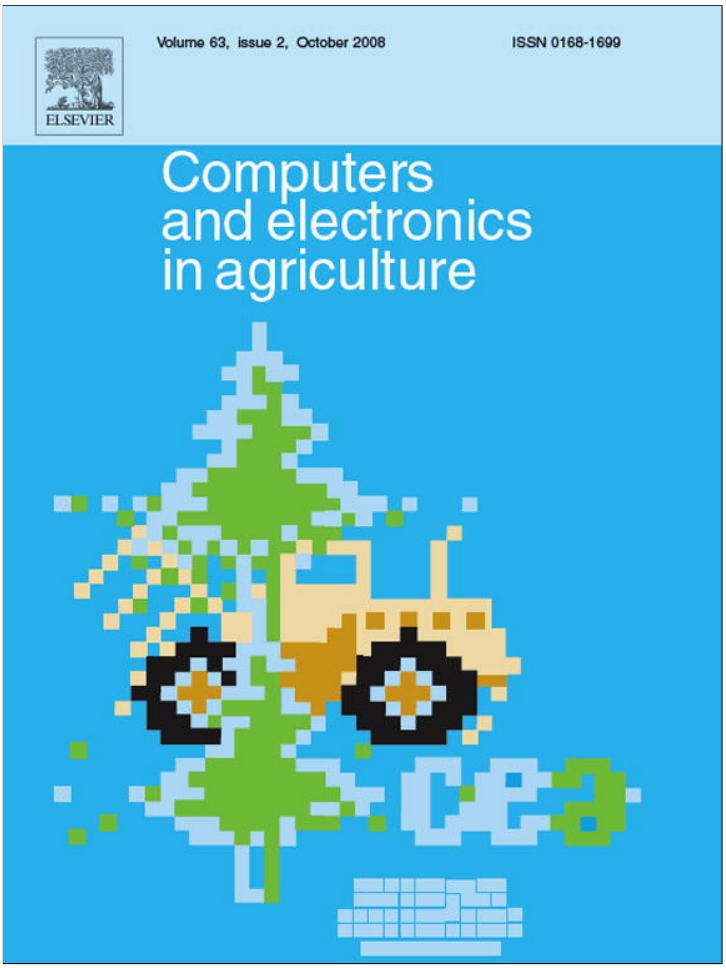

COMPUTERS AND ELECTRONICS IN AGRICULTURE 63 (2008) 245–256

available at www.sciencedirect.com

ScienceDirect

journal homepage: www.elsevier.com/locate/compag

# Propagation of positional measurement errors to agricultural field boundaries and associated costs

*S. de Bruin*[a,*], *G.B.M. Heuvelink*[b], *J.D. Brown*[c]

[a] *Wageningen University, Centre for Geo-Information, PO Box 47, 6700 AA Wageningen, The Netherlands*
[b] *Wageningen University, Landscape Centre, Wageningen, The Netherlands*
[c] *National Weather Service, N.O.A.A., Silver Spring, MD, USA*

ARTICLE INFO

*Article history:*
Received 17 October 2007
Received in revised form
11 March 2008
Accepted 17 March 2008

*Keywords:*
GPS
Path planning
Geostatistics
Temporal correlation
Stochastic simulation
GIS

ABSTRACT

It has been argued that the upcoming targeted approach to managing field operations, or precision farming, requires that field boundaries are measured with cm level accuracy, thus avoiding losses such as wasted inputs, unharvested crops and inefficient use of the land. This paper demonstrates a method for verification of such claims, based on a statistical model that accounts for temporal correlation in positional measurement errors. Our implementation employs the Data Uncertainty Engine (DUE), which is free software that aids the user in defining probability distributions for uncertain spatial objects, and draws random samples from these distributions. A case study concerning the financial consequences of uncertain geometry for a farmer who uses a digital map to optimise field operations for 15 ha of a potato crop is presented. The error model was parameterised on measurement scenarios representing (1) the Dutch registry of agricultural fields; (2) differential GPS-based field checks for verification of area declarations; and (3) special purpose Real Time Kinematic (RTK)-GPS surveys. We found that a farmer who has a manually digitised map of the study area would benefit from a RTK-GPS survey in a single crop year if the survey would cost less than € 442. An independent test case showed that the results of the error model were consistent with field data.



## 1. Introduction

Higher costs of chemicals, environmental awareness, technological advances and more affordable equipment have contributed to the increased popularity of automated vehicle navigation in agriculture (Keicher and Seufert, 2000; Auernhammer, 2001; Cox, 2002; Nijland, 2006). Potential benefits of these systems include reduced overlap between adjacent spray paths, resulting in less agrochemical pollution, faster operation of equipment, less operator fatigue, the ability to operate equipment in low light conditions and reduced soil compaction if field traffic is restricted to predetermined lanes (Earl et al., 2000; Chamen et al., 2003; Batte and Ehsani, 2006). Research in the area of automated farm vehicle navigation has focussed mainly on the tracking of predetermined paths (Vougioukas et al., 2006). Though several techniques have been studied (Keicher and Seufert, 2000; Reid et al., 2000), most, if not all commercially available navigation systems for farm vehicles are based on GPS (Batte and Ehsani, 2006).

Agricultural navigation systems typically employ a parallel swathing method which enables the farmer to follow a specified swath width across the entire field. First, an A–B

* *Corresponding author*. Tel.: +31 317 481830; fax: +31 317 419000.
E-mail addresses: sytze.debruin@wur.nl (S. de Bruin), gerard.heuvelink@wur.nl (G.B.M. Heuvelink), james.d.brown@noaa.gov (J.D. Brown).
0168-1699/$ – see front matter © 2008 Elsevier B.V. All rights reserved.
doi:10.1016/j.compag.2008.03.005

**Table 1 – Description of stationary GPS measurement series**

| Dataset | Rover receiver | Correction | Location (Latlon, ETRS89) | Date and time (UTC)[a] | |
|---|---|---|---|---|---|
| | | | | Start | End |
| WU-RTK | Trimble 4800 | RTK: Trimble 4700 | Wageningen, Netherlands (51 59.29′N 05 39.95′E) | May 24, 2007, 09:44:13 | May 24, 2007, 12:08:31 |
| 06-GPS-RTK | 06-GPS monitor station | RTK: 06-GPS network | Sliedrecht, Netherlands (51 49.67′N 04 47.68′E) | December 16, 2006, 07:00:00 | December 16, 2006, 11:59:59 |
| OmniSTAR-VBS | OmniSTAR 8200HP in VBS mode | OmniSTAR VBS | Wageningen, Netherlands (51 59.23′N 05 39.97′E) | July 23, 2007, 08:57:08 | July 23, 2007, 14:41:35 |
| WU-EGNOS | Trimble GeoXT | EGNOS | Wageningen, Netherlands (51 59.23′N 05 39.97′E) | July 23, 2007, 08:57:07 | July 23, 2007, 14:41:35 |
| JRC-EGNOS | CSI DGPSMax | EGNOS | Ispra, Italy (45 48.64′N 08 37.71′E) | August 25, 2007, 00:00:01 | September 03, 2007, 23:59:59 |

[a] All data except WU-EGNOS were acquired at 1 Hz sampling rate; the WU-EGNOS data were acquired at 0.5 Hz sampling rate.




**Fig. 1 – Time-coded European geostationary navigation overlay service (EGNOS) corrected GPS positions acquired at a fixed location over a period of 2 h. Observations close in time (similar grey shade) are more or less spatially clustered, which is indicative of temporal correlation.**

line is recorded on the first straight pass; next, the remaining passes are determined by the system (Sullivan and Ehsani, 2002). Depending on the available options, the approach may be combined with an initial pass around the outside edge of a field. Research in robotics has shown that coverage planning using a map, i.e. planning a path that passes over all points on a mapped surface by minimising some cost function, can be more efficient (Choset, 2001). For example, in agriculture it could allow equipment operators to adjust the working width of machines such that a field will be entirely covered in an integer number of swaths. On the contrary, in case field geometry is not known or approximately known, inefficient use of resources may be discovered too late.

The problem of automated coverage planning for farm operations has received relatively little attention (see Oksanen

et al., 2005; Jin and Tang, 2006; Taïx et al., 2006 for examples). In practice, considerable effort is required before the technology can be incorporated into integrated farm management systems (Vougioukas et al., 2006). However, in the current work we assume that such technology will become available and will allow a farmer to optimise row crop operations based on the mapped geometry of a field. The problem considered is that of sub-optimal field use caused by the propagation of positional measurement errors to mapped field boundaries and finally to the field operations map. It has been argued that targeted approaches to managing field operations requires field boundaries to be specified with cm level accuracy, thus avoiding losses such as wasted inputs, unharvested crops and inefficient use of the land (Chan et al., 2002). The aim of this work is to demonstrate a method for experimental verification of such claims, given the positional measurement approaches such as used for agricultural purposes.

Our method employs a statistical model to account for the temporal correlation in positional measurement errors (see Bogaert et al., 2005 also). Such correlations are acknowledged by manufacturers of agricultural navigation systems, who list different values for track-to-track accuracy and absolute accuracy of GPS receivers. Such temporal correlation can also be appreciated in Fig. 1, which shows spatial clustering in a series of time-coded GPS positions acquired at a fixed point. We parameterise the error model on measurement scenarios that range from manual digitising from aerial photography through satellite-based differential GPS to Real Time Kinematic (RTK)-GPS surveying. The scenarios were chosen to represent map accuracies similar to that of (1) the Dutch registry of agricultural fields and nature areas which is used as basis for agricultural declarations; (2) field checks done for verification of such declarations; and (3) special purpose surveys. Our error propagation analyses proceed to the level of financial loss for a farmer who uses the maps for optimising field operations for a potato crop, which is one of the main row crops in the Netherlands.

## 2. Methods

### 2.1. General error model

Methods for defining positional uncertainties in geographic objects include partial and full applications of probability theory to vector data. They range in complexity from the simple 'epsilon ($\varepsilon$) band' approach, where a buffer of radius $\varepsilon$ is imposed around each line segment, to the distortion of lines and polygons with an autocorrelated 'shock' (Kiiveri, 1997), and the estimation of joint probability distribution functions for the elementary vertices of line segments, which include the spatial correlation between the positional errors of the vertices. Following the latter approach and ignoring uncertainty caused by sampling and approximation of a curvilinear feature by a sequence of straight line segments (De Bruin, in press), the positional uncertainty of area objects in a GIS is expressed as a function of uncertainty in the coordinates of their elementary vertices (Shi and Liu, 2000; Zhang and Kirby, 2000; Bogaert et al., 2005; Heuvelink et al., 2007). The coordinates of vertices (e.g. corner points) are subject to observational error

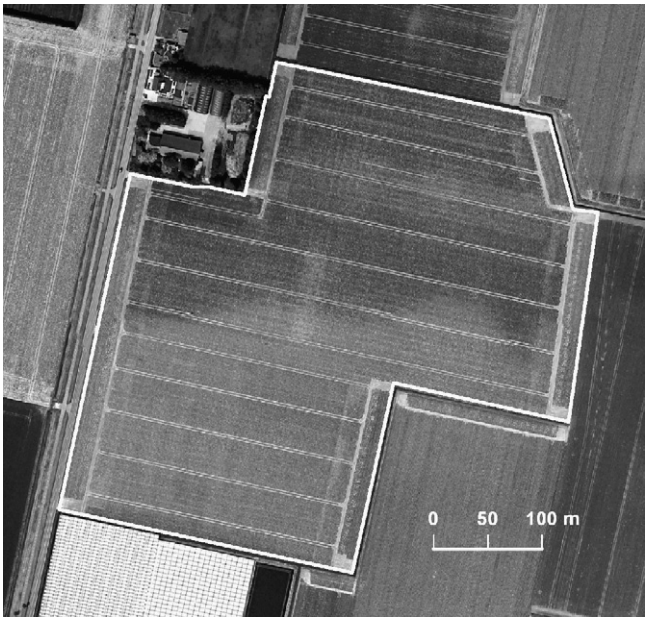


**Fig. 2 – Case study: potato field of 15 ha in the Hoeksche Waard, The Netherlands.**

which in 2D Cartesian space can be represented by the random variables $X$ and $Y$, with marginal (cumulative) probability distribution functions (mpdfs) $F_X$ and $F_Y$ (Eq. (1)):

$$F_X(x) = \text{Prob}(X \leq x) \quad \text{and} \quad F_Y(y) = \text{Prob}(Y \leq y) \tag{1}$$

where $x$ and $y$ are real numbers. When the errors in the $x$- and $y$-direction are correlated, the joint pdf is required (Eq. (2)):

$$F_{XY}(x, y) = \text{Prob}(X \leq x \text{ and } Y \leq y) \tag{2}$$

The expectations (means) $\mu_X$ and $\mu_Y$ can be estimated using repeated measurement at a location with known coordinates to provide information on positional bias. The standard deviations $\sigma_X$ and $\sigma_Y$ of $X$ and $Y$ that can easily be computed from $F_{XY}$ are measures of the random positional uncertainty in the $x$ and $y$ errors, respectively. A spatial object is treated as 'deformable' if its component vertices can move with a degree of independence (Brown and Heuvelink, 2007; Heuvelink et al., 2007). Description of the positional uncertainty of a deformable object composed of $n$ vertices requires a $2n$-dimensional joint probability distribution function (jpdf). This jpdf contains the mpdfs for the coordinates of the individual vertices, together with all the auto- and cross-correlations between them (Eq. (3)):

$$F_{X_1Y_1,\ldots,X_nY_n}(x_1, y_1, \ldots, x_n, y_n) = \text{Prob}(X_1 \leq x_1, Y_1 \leq y_1, \ldots, X_n \leq x_n, Y_n \leq y_n) \tag{3}$$

Data collection methods used to produce vector datasets (e.g. GPS surveys and manual digitising) may introduce temporal correlations of measurement errors, and these will affect the correlations represented in Eq. (3).

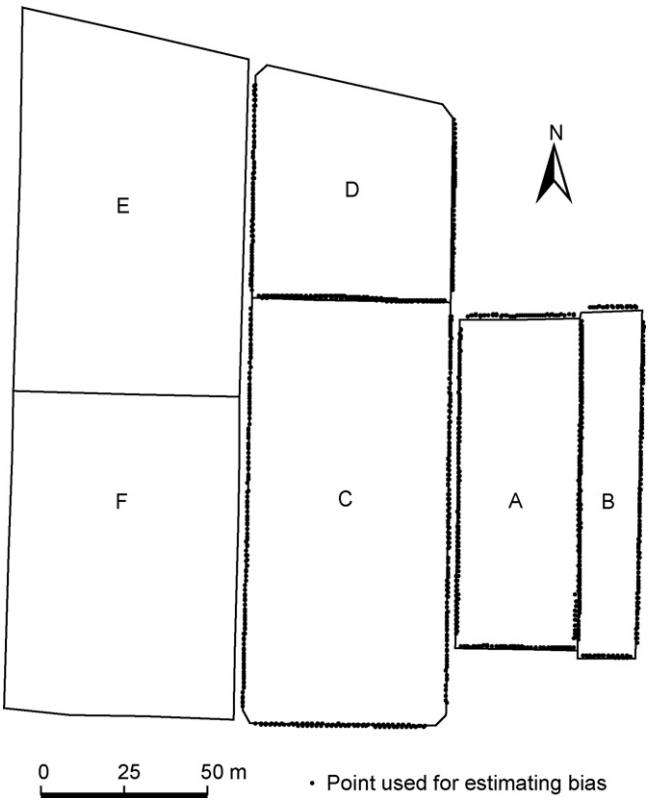


**Fig. 3 – Test plots E and F for the error model with EGNOS scenarios. Plots A–D were used for assessing positional bias in the GPS measurements.**

As a simplification of Eq. (3), a 'rigid' object contains multiple vertices whose relative positions do not change under uncertainty (Brown and Heuvelink, 2007; Heuvelink et al., 2007). Examples of rigid objects might include buildings whose boundaries are theoretically rigid or fields whose boundaries are treated as rigid for simplicity. The positional uncertainty of a rigid object can be characterised completely by a translation and possibly rotation of the object about a single point.

### 2.2. *Estimation*

Estimation of Eq. (3) typically relies on the assumption of second-order stationarity, whereby the second-order properties of the positional errors (expectations and covariances) do not vary under translation. This usually involves modelling with a joint normal distribution, which is completely defined by its means and covariances, and a covariance function that depends only on the relative distances between points (Goovaerts, 1997; Heuvelink et al., 2007).

Geostatistical error models usually consider spatial correlations of random variables. These spatial correlations may be driven by spatial processes, such as variations in terrain or soil properties, or may be caused by short-term temporal variations, such as changes in satellite clock errors, orbit errors, atmospheric delays and filtering by the GPS receiver (Bona, 2000; Olynik et al., 2002; Amiri-Simkooei and Tiberius, 2007). Likewise, manual digitisation of polygons is a sequential procedure that may result in temporal correlations among errors if consecutive vertices are digitised with similar deviations. It is usually more straightforward and realistic to model these temporal correlations than the resulting spatial correlations, as the temporal lag between the recordings is the main driver of the correlation. Therefore, our error model considers temporal correlation of positional errors. These were described by temporal semivariograms (Eq. (4)), which under second-order stationarity are related to correlograms (Eq. (5)), for example:

$$\gamma_X(\tau) = \tfrac{1}{2}\mathrm{Var}[X(t+\tau) - X(t)] \quad (4)$$

$$\rho_X(\tau) = \frac{1 - \gamma_X(\tau)}{\sigma_X^2} \quad (5)$$

where $t$ is time, $\tau$ is a time lag and $\rho_X(\tau)$, $\gamma_X(\tau)$, and $\sigma_X^2$ are the correlogram, the semivariogram and the variance of positional errors in $x$-direction, respectively. The same functions can be defined in the $y$-direction, whereas a cross-semivariogram $\gamma_{XY}(\tau)$ would be needed to characterise the cross-correlation between positional errors in the $x$- and $y$-directions.

Semivariogram analysis of the experimental data described below was performed using the Gstat geostatistical software (Pebesma and Wesseling, 1998; Pebesma, 2004). In the case of cross-correlations between the $x$ and $y$ errors, a linear model of co-regionalisation was used (Goovaerts, 1997), as this guarantees a valid covariance structure. Similar to (Bogaert et al., 2005), we assumed the errors to be normally distributed. However, unlike that work, we allow for different variances for the GPS errors in the $x$ and $y$ directions, while maintaining a stationary correlation function. In this context, the GPS satellite orbits cross the equator with an angle of 55°, which reduces the signal availability from the northern ($y$) direction in the Netherlands (52°N latitude).

### 2.3. *Data and scenarios*

Table 1 lists the GPS datasets that were used to parameterise several measurement scenarios for our error model. The first two (WU-RTK and 06-GPS-RTK) comprise survey-quality data acquired with dual frequency (L1 and L2) carrier phase RTK-GPS equipment. The former were acquired in Wageningen using a single base station and a roving receiver on a short base line. The latter comprise data from a company (06-GPS) providing RTK correction signals from a network solution based on reference stations in the Netherlands, Germany and Belgium via cell phone (Henry and Polman, 2003).

The lower three rows of Table 1 present single frequency (L1) code phase GPS data, with differential correction based on networks of widely spaced reference stations and transmitted by geostationary satellites. These data are comparable to the data used for GPS-based verification of area claims by farmers applying for subsidy under the European Union Common Agricultural Policy (CAP) (Bogaert et al., 2005). OmniSTAR-VBS (Virtual Base Station) corrections are provided on a subscription basis to give a horizontal accuracy better than 1 m (Visser, 2007). OmniSTAR also provides a High Performance (HP) dual frequency DGPS service giving decimetre level accuracy, but this was not used in the present study. European geostationary

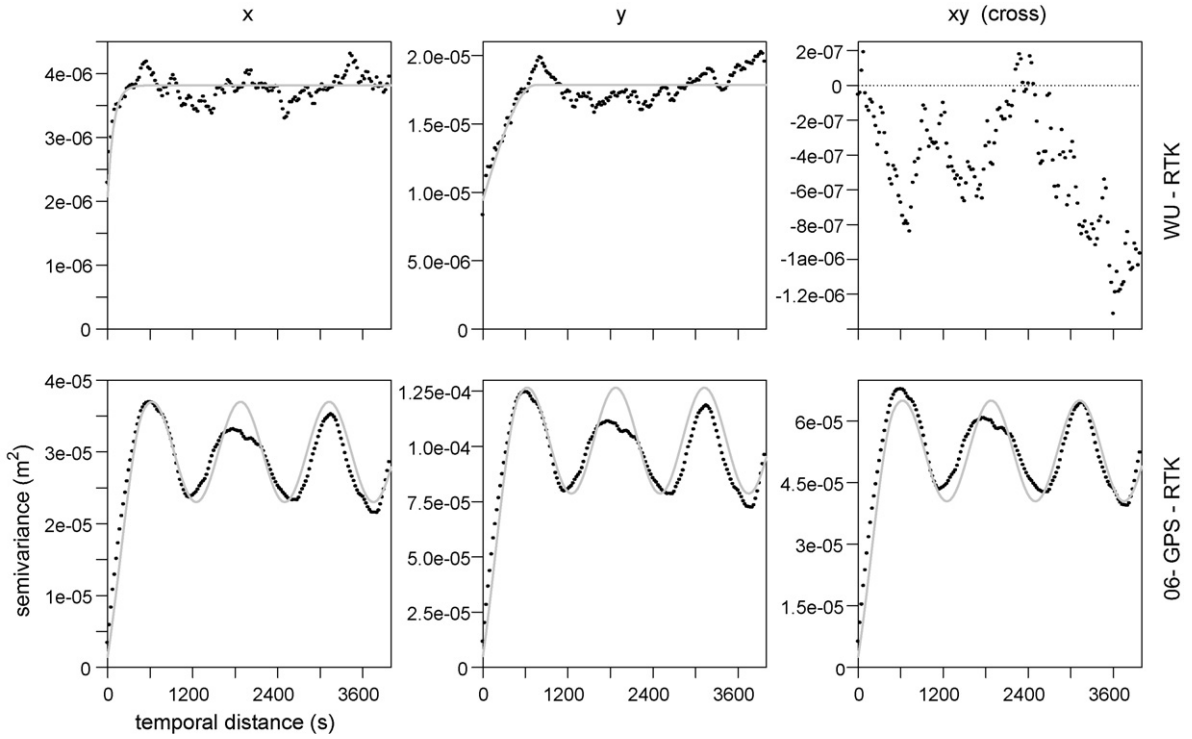


**Fig. 4 – Semivariograms and cross-variograms of the RTK-GPS data. Fitted models are indicated by grey lines; the dots represent experimental data. Note that the scale of the y-axis differs from plot to plot.**

navigation overlay service (EGNOS) provides free differential and integrity signals aiming to enhance GPS accuracy (Gauthier et al., 2001). The data provided by JRC (see Table 1) were acquired over a continuous period of 10 days. This allowed us to model temporal correlations of GPS errors over several hours as well as over several days. The EGNOS augmented data were acquired while the system was still in a pre-operational phase. All data were acquired at fixed positions.

In addition, two scenarios for data acquisition by manual digitising were considered, namely a 'rigid object' scenario and a 'deformable object' scenario. Deformity of the field boundaries under positional measurement error is more realistic than rigid movement when dealing with multiple error sources, but is also more difficult to model. For the rigid object scenario, and based on Van Buren et al. (2003), we assumed zero mean positional errors in x- and y-direction, with a standard deviation of 2 m in each direction ($\sigma_X = \sigma_Y = 2$ m) and no cross-correlation. For the deformable object scenario, we adopted the same standard deviations and analysed variography of positional errors in manually digitised vertices of a potato field (see Fig. 2) to assess temporal correlation of the errors. To this end, the field was digitised five times at a speed of approximately 1 vertex per 2 s, using a backdrop of a digital orthophoto with a resolution of 0.5 m and reference geometry, displayed at a scale of 1:4300 on a monitor with a pixel pitch of 0.297 mm.

Both scenarios aim to represent the accuracy of the Dutch registry of agricultural fields and nature areas, which is largely derived from the Top10Vector digital topographic dataset (Hoogerwerf et al., 2003). While the deformable object case emphasizes human digitising errors, the rigid object case focuses on positional errors due to incorrect alignment of orthophotography.

### 2.4. *Case study*

Fig. 2 shows our case study, a potato field of 15 ha in the Hoeksche Waard, The Netherlands. The ($x_i$, $y_i$) coordinates in the Dutch grid system of the $n = 14$ corner points of this field were measured by a professional surveyor using RTK-GPS equipment. The resulting coordinates and mapped field boundaries were used as the reference geometry in the present work. By construction, any observation error in these locations is of no consequence for our results, because the reference geometry constitutes our 'true' geometry in all subsequent calculations.

Under any of the considered measurement scenarios, however, the coordinates of vertices are subject to observational error. For the RTK-GPS and the manual digitizing scenarios referred to in Table 1, these errors were considered at the original 14 corner points. For the DGPS scenarios we emulated the common practice for GPS-based verification of area declarations under the CAP, where an operator walks around the field while GPS positions are acquired at a rate of 1 Hz. Therefore, the number of vertices was increased to 1 per 1.4 m ($n_{DGPS} = 1258$).

### 2.5. *Simulation and overlay*

The Data Uncertainty Engine (DUE) Version 3.1 (Brown and Heuvelink, 2007) was used for generating 250 realisations of

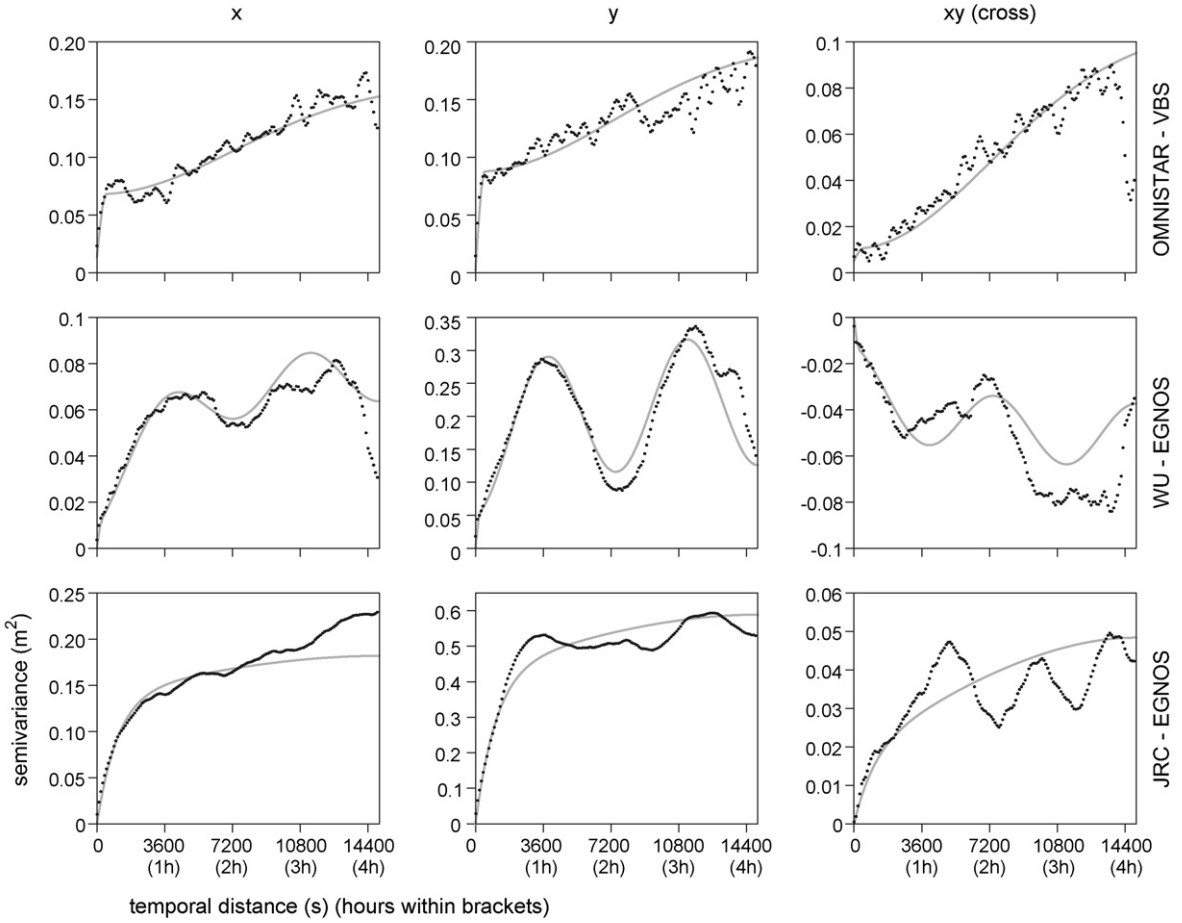


**Fig. 5 – Semivariograms and cross-variograms of the DGPS data. Fitted models are indicated by grey lines; the dots represent experimental data. Note that the scale of the y-axis may differ from plot to plot.**

the error model with parameterisations representing each of the measurement scenarios described above. DUE is free software that aids the user in defining probability distributions for uncertain spatial objects and draws random samples from these distributions. In all cases we assumed normally distributed errors with zero bias and the standard deviations ($\sigma$) were assessed by the square root of the sill (constant maximum level) of the semivariograms. Note that positional bias (if present) can be compensated for after repeated measurement of points with known positions. The analyses involved time series of either 14 (RTK-GPS and topographic map) or 1258 (DGPS) point positions. The corresponding time values were chosen to represent an operator who walks around the field from one point to the next (DGPS) or they were separated by 2 s (manual digitising).

In DUE, sampling from the joint-normal distribution is first attempted by factorising the covariance matrix $\Sigma$, giving $L$, such that $\Sigma = LL^{T}$, where T represents the transpose. Secondly, a vector of samples is obtained from the standard Normal distribution $N(0, I)$, with covariance matrix equal to the identity matrix $I$. Sampling from the pdf then involves rescaling by $L$, and adding the vector of means $\mu$ (Eq. (6)):

$$x = \mu + Lz \quad (6)$$

where z is a random sample from $N(0, I)$ and x is a random sample from the required distribution $N(\mu, \Sigma)$. If $\Sigma$ is too large to factorise, a sequential simulation algorithm is called from Gstat within DUE (Brown and Heuvelink, 2007).

The next 'stochastic simulation' or 'Monte Carlo' step involved estimating the probability distributions of the consequences of uncertainty in the vertex positions. The realized time series of positional measurements were converted into polygons and any self-intersections of the boundaries were removed by deleting small sliver polygons. The resulting polygons were geometrically intersected with the reference field using ArcGIS® 9 software. Two types of error were considered in the intersections:

1. False inclusions (errors of commission); areas outside the field geometry that are erroneously mapped as belonging to the field.
2. False exclusions (errors of omission); areas belonging to the reference field that are erroneously excluded from the mapped field.

In the first case, the farmer will plan field operations outside the true field; in the second case, the farmer will subutilize the field because part is left uncultivated.

**Table 2 – Semivariogram models fitted using the linear model of co-regionalisation specified using Gstat[a] notation**

| Scenario | x | y | xy (cross) |
|---|---|---|---|
| WU-RTK | 2.08E−06 Nug(0) + 1.74E−06 Exp(85.2) | 9.46E−06 Nug(0) + 8.38E−06 Sph(739) | 0 |
| 06-GPS-RTK | 1.50E−06 Nug(0) + 2.15E−05 (500) + 7.00E−06 Per(1250) | 5.13E−06 Nug(0) + 7.35E−05 Sph(500) + 2.40E−05 Per(1250) | 2.64E−06 Nug(0) + 3.78E−05 Sph(500) + 1.23E−05 Per(1250) |
| OmniSTAR-VBS | 0.0137 Nug(0) + 0.0542 Sph(481) + 0.0964 Gau(10311) | 0.00194 Nug(0) + 0.0855 Sph(481) + 0.1124 Gau(10311) | 0.00516 Nug(0) + 0.00523 Sph(481) + 0.0964 Gau(10311) |
| WU-EGNOS | 0.00872 Sph(250) + 0.0563 Exp(4000) + 0.0115 Per(7500) | 0.0485 Sph(250) + 0.0794 Exp(4000) + 0.0967 Per(7500) | −0.0120 Sph(250) − 0.026 Exp(4000) − 0.0136 Per(7500) |
| JRC-EGNOS | 0.141 Exp(1100) + 0.0409 Sph(15000) | 0.436 Exp(1100) + 0.153 Sph(15000) | 0.0194 Exp(1100) + 0.0290 Sph(15000) |
| JRC-EGNOS$^{long}$ | 0.147 Exp(1100) + 0.0398 Per(43082) + 0.0225 Per(86164) | 0.470 Exp(1100) + 0.0925 Per(86164) | 0.0263 Exp(1100) + 0.0353 Per(86164) |
| Manual digitizing[b] | 4 Nug(0) | 4 Nug(0) | 0 |

[a] Exp = exponential structure, Gau = Gaussian structure, Nug = nugget, Per = periodic structure, Sph = spherical structure; within brackets the range in seconds.
[b] Deformable object; in case of a rigid object, $\sigma_X = \sigma_Y = 2$ m, cov(X, Y) = 0 and the errors at the individual vertices are fully correlated, i.e. the object is displaced as a whole.

### 2.6. *Financial loss*

The errors listed above will have financial consequences if a farmer fully relies on measured field geometry for planning and performing field operations. To assess these, we considered a potato crop and used costs and net result data from PPO (2006) for a clay soil in the South West of The Netherlands. For error type 1 (errors of commission) areas, we assumed that the crop would be lost, while certain costs are made. This could be the case, for example, if inputs are supplied to a trail along the field, where the crop will be damaged by vehicles. The futilely used inputs (seed–potato, fertilizers, fungicides, herbicides, insecticides, fuel, soil analyses, interest and crop insurance) would entail a loss of € 0.1923 $m^{-2}$. This loss would be higher if the costs of labour and wear of machinery were also included. Additionally, there are risks of damage to equipment and to the environment but these are not considered here.

Errors of type 2 (errors of omission) were assumed to imply loss of net income; so input costs (see above) are saved but also no crop is harvested. Accordingly, areas with type 2 error were multiplied with the net return rates (€ 0.2023 $m^{-2}$) listed in PPO (2006). In contrast to the loss associated with type 1 errors, this loss would be *lower* if the costs of labour and wear of machinery were included.

### 2.7. *Test*

To check the error model and its parameterisation for the EGNOS scenarios, we performed an experiment using EGNOS augmented measurements of test plots acquired by a professional controller during the 2007 GPS workshop of the Joint Research Centre (JRC) of the European Commission. The operator measured six plots (see Fig. 3) in duplicate using an EGNOS enabled GPS receiver by collecting point positions at 1 Hz, while walking along clearly observable boundaries that were also marked by pickets. Points collected along the East – West and North – South oriented boundaries of plots A–D were used to assess positional bias in the GPS data. After correcting for bias, the measured geometries of plots E and F were intersected with reference geometry acquired using RTK-GPS equipment and the false inclusion and false exclusion areas were calculated. The reference areas of plots E and F were 7362 and 6612 $m^2$, respectively. Measurement errors in the RTK-GPS reference data were ignored in this test.

Simulated areas with either type of error were obtained using the error model and the EGNOS scenarios listed in Table 1. Probabilities of exceedance of the measured areas were estimated by the fraction of simulated areas that were above the measured areas. These give the probability of obtaining false inclusion and false exclusion areas larger than the measured values, according to the error model and measurement scenario. Values close to 1 or 0 would, therefore, indicate that it is very unlikely to obtain similar values with the specific model set-up. It is worthwhile noting, however, that in addition to uncertainty in the GPS measurements, the field data were likely to be influenced by other sources of error, such as uncontrolled movement of the antenna during data acquisition.

**Table 3 – Summary statistics of areas in error ($m^2$) under various scenarios**

| Scenario | Error | Mean | SD | Percentile | |
|---|---|---|---|---|---|
| | | | | $P_{10}$ | $P_{90}$ |
| WU-RTK (corners) | Commission | 2.40 | 1.05 | 1.42 | 3.66 |
| | Omission | 3.83 | 0.86 | 2.99 | 5.05 |
| 06-GPS-RTK (corners) | Commission | 6.02 | 3.54 | 2.08 | 10.9 |
| | Omission | 5.99 | 3.01 | 3.25 | 9.38 |
| OmniSTAR-VBS (continuous, 1 Hz) | Commission | 304 | 146 | 138 | 502 |
| | Omission | 306 | 162 | 132 | 503 |
| WU-EGNOS (continuous, 1 Hz) | Commission | 261 | 115 | 129 | 414 |
| | Omission | 262 | 117 | 130 | 446 |
| JRC-EGNOS (continuous, 1 Hz) | Commission | 383 | 175 | 172 | 609 |
| | Omission | 384 | 179 | 168 | 606 |
| JRC-GNOS$^{long}$ (continuous, 1 Hz) | Commission | 410 | 197 | 167 | 683 |
| | Omission | 400 | 215 | 159 | 680 |
| Manual digitizing[a] (corners) | Commission | 1127 | 504 | 512 | 1758 |
| | Omission | 1122 | 480 | 529 | 1787 |
| Manual digitizing[b] (rigid object) | Commission | 1409 | 709 | 557 | 2394 |
| | Omission | 1410 | 709 | 558 | 2395 |

[a] Deformable object.
[b] Rigid object.

## 3. Results and discussion

### 3.1. *Semivariograms*

Figs. 4–6 show the experimental semivariograms and fitted models for the RTK-GPS data, the DGPS data and the JRC-EGNOS data with time lags extending more than 5 days, respectively. The parameters of the semivariogram models fitted under the linear model of co-regionalisation are listed in Table 2.

Temporal cross-correlation between x and y errors in the WU-RTK data was ignored because of its small magnitude and erratic structure (upper right of Fig. 4). The 06-GPS-RTK

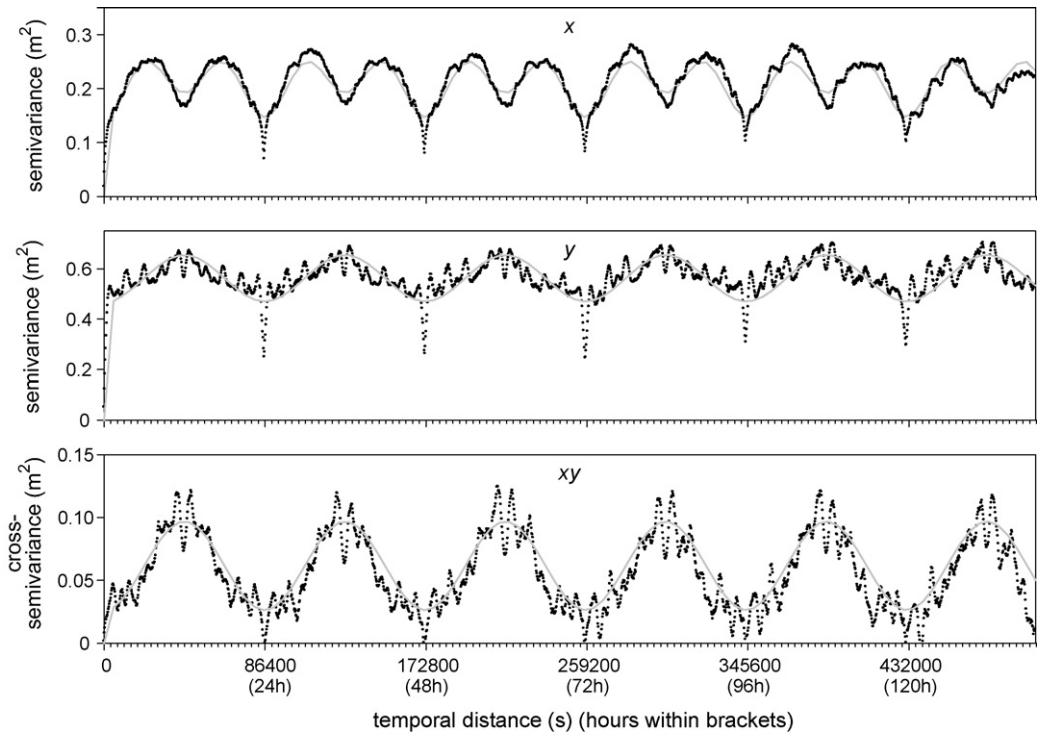


**Fig. 6 – Semivariograms and cross-variograms of the JRC-EGNOS data, with extended time lags.**

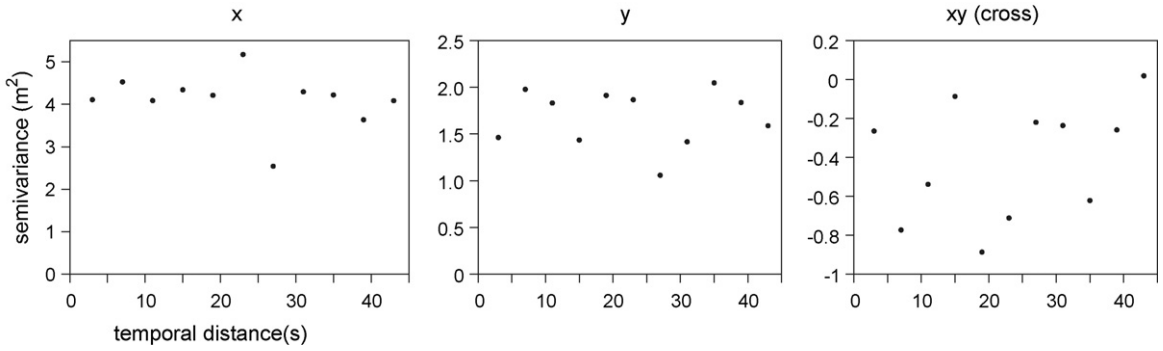


**Fig. 7 – Experimental semivariograms of manual digitising errors, showing no temporal correlation.**

semivariograms (lower row Fig. 4) show remarkable periodicity possibly caused by incompletely removed multipath effects at the monitor station (rover) or somewhere in the network (recall that 06-GPS provides a network solution). Multipath effects happen when a GPS unit receives both the direct GPS signal and signals reflected by e.g. buildings. It differs from site to site and from time to time as it depends on the azimuth and elevation of the satellites and local geometry, i.e. obstacles in close proximity to the measured location (Amiri-Simkooei and Tiberius, 2007).

A comparison of the lowest row of Figs. 5 and 6 (EGNOS augmented GPS data) illustrates that semivariograms of GPS observations with time lags up to just a few hours may underestimate variance and miss relevant periodicity. The main period (86,164 s, see Table 2) corresponds with the nominal (sidereal) period over which the GPS satellites complete two orbits and the Earth completes one revolution, so that the constellation returns to the same geometry (Agnew and Larson, 2007). Diurnal atmospheric effects are assumed to be compensated by the correction signal.

Note that our EGNOS variography is notably different from the structure reported by Bogaert et al. (2005). The latter only comprised a single Gaussian structure with an effective range of 30 s and a sill of 6.8 $m^2$, which is rather high in comparison to the accuracy that is claimed to be possible with EGNOS augmentation. Obviously, there is no single semivariogram that can be used for all EGNOS enabled GPS receivers under all circumstances. Therefore, our parameterisations of the error model should not be used uncritically beyond the scenarios presented here.

The semivariograms of the manual digitising errors (Fig. 7) reveal no clear patterns of temporal correlation. Therefore, the direct semivariograms were modelled by nugget structures and based on Van Buren et al. (2003) the sills for both $x$ and $y$ were set at 4 $m^2$. Temporal cross-correlation between $x$ and $y$ errors in the manually digitised data was ignored because of its small magnitude and erratic structure.

### 3.2. *Area uncertainty*

All simulations were performed on a Pentium PC with 2.5 GB RAM, and the DUE 3.1 simulations were achieved by factorisation of the covariance matrix, using the full jpdf (Eq. (6)). For the WU-EGNOS scenario, we used sequential Gaussian simulation in Gstat, because negative cross-correlations are not currently supported in DUE. Fig. 8 shows an overlay of a realisation of the manual digitising/deformable object scenario with the reference field, indicating areas with either of the two types of error. If the farmer would rely on this manually digitised map to plan field operations, in the North he would leave a large strip uncultivated while in the South his plans would partly cover a ditch. Summary statistics of the areas in error for all scenarios resulting from 250 realisations each are listed in Table 3. Not surprisingly, the mean areas incorrectly mapped are approximately proportional to the standard deviations of the positional errors for each type of error. On the other hand, the non-Gaussian distributions of the histograms (not shown here for brevity) are symptomatic of the non-linear operation performed on the data. This explains the utility of Monte Carlo simulation, which can be applied to any type of model.

### 3.3. *Financial losses*

Table 4 lists the summary statistics of the financial losses suffered by the farmer in a single year if the measured geometry was used to plan and execute field operations for a potato crop.

For the 15-ha potato field considered here, a manually digitised map would involve an expected loss greater than € 443 with respect to the 'true' geometry. In the deformable object case, there is 10% probability that this loss would exceed €

**Table 4 – Summary statistics of financial loss (€) with respect to error-free geometry under various scenarios**

| Scenario | Mean | SD | Percentile | |
|---|---|---|---|---|
| | | | $P_{10}$ | $P_{90}$ |
| WU-RTK | 1.24 | 0.19 | 1.06 | 1.45 |
| 06-GPS-RTK | 2.37 | 0.85 | 1.53 | 3.48 |
| OmniSTAR-VBS | 120.36 | 53.17 | 65.27 | 196.99 |
| WU-EGNOS | 103.19 | 39.92 | 62.22 | 164.36 |
| JRC-EGNOS | 151.18 | 56.50 | 84.56 | 220.27 |
| JRC-EGNOS$^{long}$ | 159.77 | 69.48 | 84.42 | 263.23 |
| Manual digitizing[a] | 443.69 | 86.66 | 343.21 | 565.20 |
| Manual digitizing[b] | 556.24 | 279.79 | 220.03 | 944.85 |

[a] Deformable object.
[b] Rigid object.

**Table 5 – Measured areas in error (after correction for positional bias) and probability of exceedance computed from 250 simulations, for the test case**

| Measured field | Measured error ($m^2$) | | Simulation scenario | Probabilities[a] | | |
|---|---|---|---|---|---|---|
| | Commission ($\varepsilon_c$) | Omission ($\varepsilon_o$) | | $P(s_c > \varepsilon_c)$ | $P(s_o > \varepsilon_o)$ | $P(s_c > \varepsilon_c, s_o > \varepsilon_o)$ |
| *E* (first measurement) | 68.4 | 48.5 | WU-EGNOS | 0.21 | 0.44 | 0.17 |
| | | | JRC-EGNOS | 0.51 | 0.75 | 0.48 |
| | | | JRC long | 0.52 | 0.72 | 0.48 |
| *E* (second measurement) | 80.2 | 51.2 | WU-EGNOS | 0.14 | 0.40 | 0.13 |
| | | | JRC-EGNOS | 0.42 | 0.72 | 0.42 |
| | | | JRC long | 0.43 | 0.72 | 0.41 |
| *F* (first measurement) | 79.8 | 16.5 | WU-EGNOS | 0.10 | 0.93 | 0.10 |
| | | | JRC-EGNOS | 0.44 | 0.98 | 0.44 |
| | | | JRC long | 0.42 | 0.95 | 0.42 |
| *F* (second measurement) | 84.3 | 15.3 | WU-EGNOS | 0.08 | 0.94 | 0.08 |
| | | | JRC-EGNOS | 0.39 | 0.98 | 0.39 |
| | | | JRC long | 0.38 | 0.96 | 0.38 |

[a] $s_c$ = simulated area with commission error; $s_o$ = simulated area with omission error.

565, while for a rigid object this is € 945. The larger spread for a rigid object is attributed to the complete correlation of measurement errors at the vertices (i.e. an extreme at one point is propagated everywhere). In contrast, in the case of a deformable object, a positive measurement error at one point can be partly compensated for by a negative error at another vertex, because the positional errors of vertices are uncorrelated. Recall that the two scenarios aim to represent human digitising errors (deformable object) and orthophotography alignment errors (rigid object).

The expected losses for the DGPS scenarios vary between € 100 and € 160 and the losses for the RTK-GPS scenarios are virtually negligible. If, for example, the farmer of the case study has a manually digitised map of his field, the cut-off point at which an RTK-GPS survey would become cost-effective is € 442 in a single crop year. Note that the GPS survey would not need to be conducted every year while benefits may persist for several years (as long as field geometry does not change). Another example: after some manipulation of the table entries it becomes apparent that there is a 99% chance that a farmer owning a manually digitised/rigid object map of the field will benefit from a map made under the EGNOS-JRC scenario.

It is important to note that the risks considered in these examples concern only the crop inputs and the yields. Other risks associated with errors of commission, such as damage to equipment and infrastructure (e.g. the risk of hitting obstacles in the field by machinery) and externalities (e.g. environmental effects) are not considered here. However, these may considerably increase the benefits of accurate mapping.

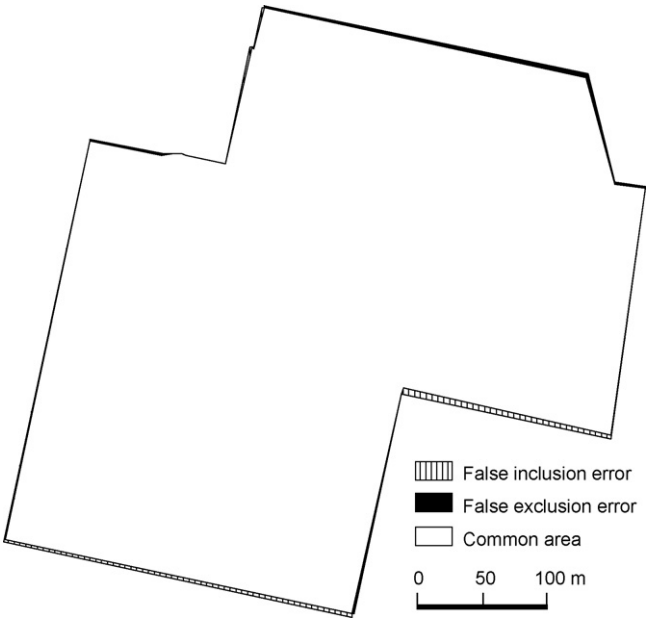


**Fig. 8 – Geometrical intersection of a realisation of the manual digitising/deformable object scenario and the reference field, indicating the two types of error.**

### 3.4. *Test*

Table 5 lists the area measurements of the test plots and their probabilities of exceedance computed from 250 realisations of the error model parameterised on the three EGNOS scenarios. Although the field measurements were influenced by other error sources in addition to the GPS measurement errors (as indicated above), for plot E, the observed areas are similar to values produced by the error model. This can be seen from the non-extreme exceedance probabilities in the upper part of Table 5. For plot F, the observed errors of omission were too small to be reproduced frequently by the error model. To find an explanation for this, it should be noted that plot E was fallow, while plot F had barley. Apparently, the operator walked somewhat outside the marked area so as not to damage the crop, and this resulted in rather large errors of commission and extremely low errors of omission.

## 4. Conclusions

We have presented a general positional error propagation method that can be used for verification of claims regarding the required positional accuracy of maps for planning field operations. Our implementation employs the DUE, which is

free software that aids the user in defining probability distributions for uncertain spatial objects and draws random samples from these distributions. In the current work we did not explicitly consider field operations (e.g. ploughing, seeding, spraying, and harvesting), but instead computed probability distributions of areas that would erroneously be included in or excluded from a plan and thus have financial consequences for a farmer. However, the method can readily be used to generate map realisations for error propagation studies involving more complex analyses.

The approach can be used to make an economic assessment for using alternative field maps. Our examples illustrate considerable differences between the losses associated with specific map accuracies, even when only direct losses for a farmer are considered. For example, a farmer who has a manually digitised map of the study area would benefit from a RTK-GPS survey in a single crop year if the survey would cost less than € 442. The expected benefits of accurate maps would most likely be larger if secondary losses (e.g. potential damage to equipment and infrastructure, environmental pollution) are also accounted for in the model.

Our semivariogram analyses of stationary GPS time series revealed substantial temporal correlation in the positional errors for several measurement set-ups involving DGPS and RTK-GPS configurations. The semivariogram models found in this study should not be used uncritically elsewhere, because the structure of temporal correlation may vary from site to site, from time to time and between receivers. However, further studies of this type may highlight consistencies between the error models generated under certain conditions.

An independent test case showed that the results of the error model with the EGNOS scenarios were consistent with field data. Differences between observed and simulated areas in error for one of the test plots are likely to be caused by an impediment during field data acquisition.

## Acknowledgements

This work was largely carried out within the project "Geo-information requirement for agri-environmental policy" which is co-financed from the program "Space for Geo-information" (Project RGI-017). We thank Fugro for facilitating a trial with OmniSTAR VBS, Jean Paul Henry for providing the 06-GPS dataset, Aleksandra Sima (JRC) for the long EGNOS time series, Lucie Šavelková and Jan Bašek for the GPS data of the test plots, Van Waterschoot Landmeetkunde for the reference geometry of the study area, Roland van Zoest who wrote a Python script for importing polygons and Philip Wenting for his help with several GPS measurements. Special thanks go to Aad Klompe (farmer in the Hoeksche Waard and chairman of H-WodKa) who introduced us to the problem setting.

## REFERENCES

Agnew, D., Larson, K., 2007. Finding the repeat times of the GPS constellation. GPS Solut. 11, 71–76.

Amiri-Simkooei, A.R., Tiberius, C.C.J.M., 2007. Assessing receiver noise using GPS short baseline time series. GPS Solut. 11, 21–35.

Auernhammer, H., 2001. Precision farming—the environmental challenge. Comput. Electron. Agric. 30, 31–43.

Batte, M.T., Ehsani, M.R., 2006. The economics of precision guidance with auto-boom control for farmer-owned agricultural sprayers. Comput. Electron. Agric. 53, 28–44.

Bogaert, P., Delinc, J., Kay, S., 2005. Assessing the error of polygonal area measurements: a general formulation with applications to agriculture. Meas. Sci. Technol. 16, 1170–1178.

Bona, P., 2000. Precision, cross correlation, and time correlation of GPS phase and code observations. GPS Solut. 4, 3–13.

Brown, J.D., Heuvelink, G.B.M., 2007. The Data Uncertainty Engine (DUE): a software tool for assessing and simulating uncertain environmental variables. Comput. Geosci. 33, 172–190.

Chamen, T., Alakukku, L., Pires, S., Sommer, C., Spoor, G., Tijink, F., Weisskopf, P., 2003. Prevention strategies for field traffic-induced subsoil compaction: a review. Part 2. Equipment and field practices. Soil Till. Res. 73, 161–174.

Chan, C.W., Schueller, J.K., Miller, W.M., Whitney, J.D., Wheaton, T.A., Cornell, J.A., 2002. Error sources on yield-based fertilizer variable rate application maps. Precis. Agric. 3, 81–94.

Choset, H., 2001. Coverage for robotics—a survey of recent results. Ann. Math. Artif. Intell. 31, 113–126.

Cox, S., 2002. Information technology: the global key to precision agriculture and sustainability. Comput. Electron. Agric. 36, 93–111.

De Bruin, S., in press. Modelling positional uncertainty of line features by accounting for stochastic deviations from straight line segments. Trans. GIS 12 (2), 165–177.

Earl, R., Thomas, G., Blackmore, B.S., 2000. The potential role of GIS in autonomous field operations. Comput. Electron. Agric. 25, 107–120.

Gauthier, L., Michel, P., Ventura-Traveset, J., Benedicto, J., 2001. EGNOS: the first step in Europe's contribution to the global navigation satellite system. ESA Bull. 105, 35–42.

Goovaerts, P., 1997. Geostatistics for Natural Resources Evaluation. Oxford University Press, New York.

Henry, P.J.A., Polman, J., 2003. GPS-netwerk operationeel in heel Nederland. Geodesia 3, 108–114.

Heuvelink, G.B.M., Brown, J.D., Van Loon, E.E., 2007. A probabilistic framework for representing and simulating uncertain environmental variables. Int. J. Geogr. Inform. Sci. 21, 497–513.

Hoogerwerf, M.R., Bulens, J.D., Stoker, J., Hamminga, W., 2003. Verificatie Kwaliteit BRP gegevensbank. Research Instituut voor de Groene Ruimte, Wageningen, Alterra.

Jin, J., Tang, L., 2006. Optimal path planning for arable farming. In: 2006 ASABE Annual International Meeting. American Society of Agricultural Engineers, Portland, Oregon.

Keicher, R., Seufert, H., 2000. Automatic guidance for agricultural vehicles in Europe. Comput. Electron. Agric. 25, 169–194.

Kiiveri, H.T., 1997. Assessing, representing and transmitting positional uncertainty in maps. Int. J. Geogr. Inform. Sci. 11, 33–52.

Nijland, D., 2006. Futuristisch boeren wordt haalbaar, want betaalbaar. VI Matrix 2006, 6–7.

Oksanen, T., Kosonen, S., Visala, A., 2005. Path planning algorithm for field traffic. In: 2005 ASAE Annual Meeting, Tampa, FL. American Society of Agricultural and Biological Engineers.

Olynik, M., Petovello, M., Cannon, M., Lachapelle, G., 2002. Temporal impact of selected GPS errors on point positioning. GPS Solut. 6, 47–57.

Pebesma, E.J., 2004. Multivariable geostatistics in S: the gstat package. Comput. Geosci. 30, 683–691.

Pebesma, E.J., Wesseling, C.G., 1998. Gstat: a program for geostatistical modelling, prediction and simulation. Comput. Geosci. 24, 17–31.

PPO (Praktijkonderzoek Plant en Omgeving), 2006. Kwantitatieve informatie akkerbouw en vollegrondsgroenteteelt 2006 (KWIN 2006). Lelystad, Praktijkonderzoek Plant en Omgeving.

Reid, J.F., Zhang, Q., Noguchi, N., Dickson, M., 2000. Agricultural automatic guidance research in North America. Comput. Electron. Agric. 25, 155–167.

Shi, W., Liu, W., 2000. A stochastic process-based model for the positional error of line segments in GIS. Int. J. Geogr. Inform. Sci. 14, 51–66.

Sullivan, M., Ehsani, M.R., 2002. GPS guidance systems—an overview of the 549 components and options. Ohio State University Extension Fact Sheet, Food, 550 Agricultural and Biological Engineering, The Ohio State University, Columbus, 2007.

Taïx, M., Souères, P., Frayssinet, H., Cordesses, L., 2006. Path planning for complete coverage with agricultural machines. In: Siciliano, B., Khatib, O., Groen, F. (Eds.), Field and Service Robotics. Springer, Berlin, pp. 549–558.

Van Buren, J., Westerik, A., Olink, E.J.H., 2003. Kwaliteit TOP10vector – De geometrische kwaliteit van het bestand TOP10vector van de Topografische Dienst, Kadaster – Concernstaf Vastgoedinformatie en Geodesie.

Visser, H., March/April 2007. OmniSTAR: a DGPS service for GIS mapping. Geomat. World, 22–24.

Vougioukas, S., Blackmore, S., Nielsen, J., Fountas, S., 2006. A two-stage optimal motion planner for autonomous agricultural vehicles. Precis. Agric. 7, 361–377.

Zhang, J., Kirby, R.P., 2000. A geostatistical approach to modelling positional errors in vector data. Trans. GIS 4, 145–159.